

# Investigation of Hybrid Silicon-Nitride/Polymer Waveguides for Second-Harmonic Generation

Volume 11, Number 3, June 2019

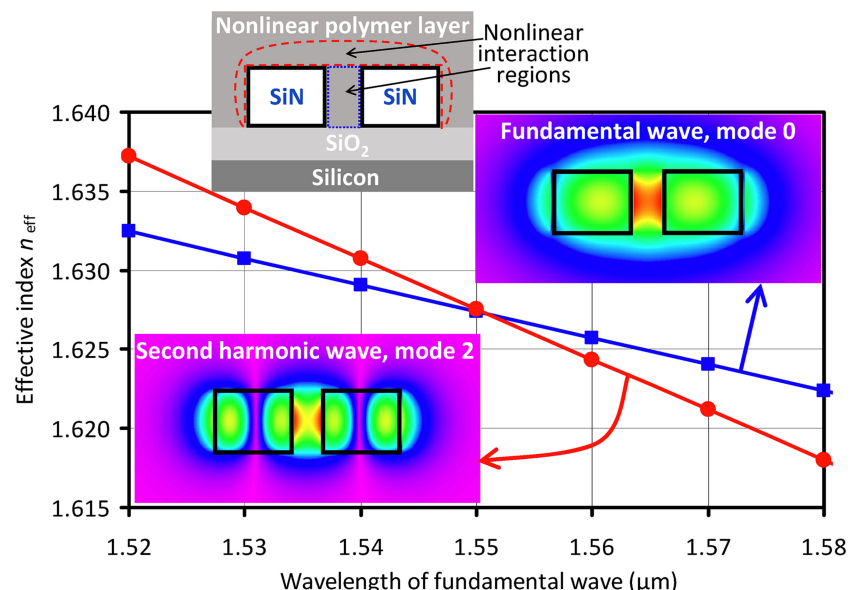
Subrata Das, *Student Member, IEEE*

Brett R. Wenner

Jeffery W. Allen, *Senior Member, IEEE*

Monica S. Allen, *Senior Member, IEEE*

Michael Vasilyev, *Senior Member, IEEE*



DOI: 10.1109/JPHOT.2019.2913551

1943-0655 © 2019 IEEE

# Investigation of Hybrid Silicon-Nitride/Polymer Waveguides for Second-Harmonic Generation

Subrata Das ,<sup>1</sup> Student Member, IEEE, Brett R. Wenner ,<sup>2</sup>  
 Jeffery W. Allen,<sup>3</sup> Senior Member, IEEE,  
 Monica S. Allen,<sup>3</sup> Senior Member, IEEE,  
 and Michael Vasilyev ,<sup>1</sup> Senior Member, IEEE

<sup>1</sup>Department of Electrical Engineering, University of Texas at Arlington, Arlington, TX 76019, USA

<sup>2</sup>Air Force Research Laboratory Sensors Directorate, Wright-Patterson Air Force Base, OH 45433, USA

<sup>3</sup>Air Force Research Laboratory Munitions Directorate, Eglin Air Force Base, FL 32542, USA

DOI:10.1109/JPHOT.2019.2913551

1943-0655 © 2019 IEEE. Translations and content mining are permitted for academic research only.  
 Personal use is also permitted, but republication/redistribution requires IEEE permission.  
 See [http://www.ieee.org/publications\\_standards/publications/rights/index.html](http://www.ieee.org/publications_standards/publications/rights/index.html) for more information.

Manuscript received February 2, 2019; revised March 19, 2019; accepted April 22, 2019. Date of publication April 26, 2019; date of current version June 17, 2019. This work was supported in part by the KBRwyle Laboratories, Inc. with Contract FA8075-14-D-0025-0005. The work of B. R. Wenner was supported by the AFRL Commander's Research and Development Fund. The work of J. W. Allen and M. S. Allen was supported by AFOSR Lab Task 17RWCOR398 (PO: Dr. K. Caster). Corresponding author: Michael Vasilyev (e-mail: vasilyev@uta.edu).

**Abstract:** We propose a hybrid silicon-nitride ( $\text{Si}_3\text{N}_4$  or SiN for short)/nonlinear polymer waveguide to achieve second-harmonic generation of an input 1550 nm signal by modal phase-matching between zero-order spatial mode at 1550 nm and second-order mode at 775 nm. We explore and optimize two cases, single channel waveguide and slot waveguide, by varying the waveguide dimensions. For TE polarized light, the optimum slot waveguide exhibits an effective interaction area  $A_{\text{eff}}$  of about  $16 \mu\text{m}^2$ , which is an order-of-magnitude improvement over the single channel waveguide and can translate to a high value of effective nonlinearity. We also show that the optimum slot waveguide geometry is robust with respect to fabrication uncertainties and bending effects.

**Index Terms:** Nonlinear integrated optics, second-harmonic generation.

## 1. Introduction

Future optical sensing, communications, and signal-processing systems will need to be compact, environmentally-robust, and energy-efficient. These requirements raise the need for on-chip integration of nonlinear-optical devices (e.g., parametric amplifiers, wavelength converters, and second-harmonic generators) with sources, detectors, and other components used in such systems. While promising  $\chi^{(3)}$ -based platforms are emerging continuously [1]–[3],  $\chi^{(3)}$  devices suffer from parasitic Raman and higher-order mixing processes degrading their noise properties (e.g., limiting the noise figure of a “noiseless” phase-sensitive amplifier to just over 1 dB [4], [5]).  $\chi^{(2)}$  interaction is free from such noises and can therefore be attractive for future low-noise-classical and quantum information processing applications [6]. However, the focus of  $\chi^{(2)}$  integrated photonics has largely remained on PPLN and PPKTP waveguides, whose inherent losses and low index contrast limit the scale of

integration. For better  $\chi^{(2)}$  integration potential, a hybrid approach combining silicon waveguides with nonlinear polymer cladding was introduced [7], [8]. However, nonlinear-optical applications of silicon-based devices are limited by the two-photon absorption (TPA). An attractive and CMOS-compatible dielectric alternative to silicon waveguides, silicon nitride ( $\text{Si}_3\text{N}_4$  or SiN for short), has high refractive index (1.9–2.0) and low absorption in both telecom / near-IR and visible wavelength ranges, which makes it possible to be used in compact photonic circuits with tight bending radii [9]–[12]. SiN also has high power-handling ability owing to negligible TPA, while exhibiting a relatively high nonlinear refractive index  $n_2$  suitable for  $\chi^{(3)}$  applications [13]–[18]. Thus, SiN waveguides and microrings can be used for both linear and  $\chi^{(3)}$ -nonlinear optics applications. On the other hand,  $\chi^{(2)}$  processes in SiN-based non-hybrid structures are limited by the central symmetry of SiN to very weak effects observable only either at the surface [19], [20] or after electric-field poling [21]. Effective  $\chi^{(2)}$  nonlinearity in SiN microrings has also been achieved in four-wave-mixing-based coherent photon conversion scheme [22].

In this paper, we describe a design of a hybrid SiN waveguide with nonlinear polymer cladding suitable for making efficient  $\chi^{(2)}$ -based devices. We use second-harmonic generation (SHG) as an example. We employ modal phase matching [23]–[25] between 0<sup>th</sup>-order mode of the near-infrared (1550-nm) fundamental wave and 2<sup>nd</sup>-order mode of the SHG wave (775 nm). This technique is similar to the one previously used in SiN-surface-based SHG [20], and it builds upon our work on multimode parametric amplification [24], [26], [27] and mode-selective wavelength conversion [25], [28]–[30]. We numerically optimize the waveguide configuration to simultaneously achieve the phase matching and maximize the nonlinear overlap integral between the interacting waves. We discussed preliminary results of this study at two conferences [31], [32]. The present paper is our complete report on full optimization of the waveguide geometry over a wide practical parameter range.

The structure of the paper is as follows. Section 2 introduces the phase-matching condition and the nonlinear overlap integral. We start by studying a single channel waveguide in Section 3, achieving the modal phase matching in both TM and TE cases. However, the nonlinear overlap in the polymer cladding region is found to be extremely small, making the single channel waveguide very inefficient for nonlinear-optical applications. In Section 4, we turn to investigation of a slot-based waveguide, and find that it meets the goals of both phase matching and maximizing nonlinear overlap integral. In Section 4.3 we also show that the slot-based waveguide is robust with respect to bending with reasonable radii down to  $\sim 150 \mu\text{m}$ , which permits its use in microresonators. Section 5 summarizes our work.

## 2. Theoretical Background

Devices that exploit second-order nonlinear effects have to meet two conditions: 1) satisfy phase matching of the interacting waves, which is necessary for accumulation of the nonlinear effects over the entire propagation distance, and 2) have a large effective nonlinearity, which is determined both by the  $\chi^{(2)}$  tensor elements of the nonlinear material and by the overlap integral of the nonlinear material and the interacting modes [25], [31]. Propagating the fundamental and SHG waves in two different waveguide modes presents an opportunity to overcome the material and waveguide dispersions and achieve perfect phase matching by making the effective refractive indices of these modes equal:

$$n_{\text{eff}}^{m,1550} = n_{\text{eff}}^{n,775}, \quad (1)$$

where  $m$  and  $n$  are the mode orders of the fundamental (wavelength  $\lambda_{1550} = 1550 \text{ nm}$ ) and SHG (wavelength  $\lambda_{775} = 775 \text{ nm}$ ) waves, respectively. Under normal dispersion conditions, typical for waveguides fabricated from relatively thin SiN films (a few hundred nm thick), the phase matching requires  $n > m$ . Once the phase-matching condition is satisfied, one needs to maximize the effective nonlinearity. For a given choice of the material with nonlinear constant  $d_{\text{eff}}$ , this means maximizing

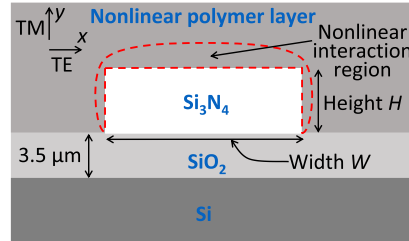


Fig. 1. Schematic of the single channel waveguide. Nonlinear  $\chi^{(2)}$  interaction occurs within the upper-cladding region with red dashed-line border.

the nonlinear overlap integral  $\Phi$  of the two interacting modes and the nonlinear material

$$\Phi = \frac{1}{A_{\text{eff}}} = \frac{\left| \int_{-\infty}^{\infty} \int_{-\infty}^{\infty} \theta(x, y) \Psi_{m, 1550}^2(x, y) \Psi_{n, 775}^*(x, y) dx dy \right|^2}{\left[ \int_{-\infty}^{\infty} \int_{-\infty}^{\infty} |\Psi_{m, 1550}(x, y)|^2 dx dy \right]^2 \int_{-\infty}^{\infty} \int_{-\infty}^{\infty} |\Psi_{n, 775}(x, y)|^2 dx dy}, \quad (2)$$

which also equals the inverse effective area  $A_{\text{eff}}$  of the SHG interaction. In Eq. (2),  $\Psi_{m, 1550}$  and  $\Psi_{n, 775}$  are the electric-field profiles of the  $m^{\text{th}}$ -order mode at  $\lambda_{1550}$  and  $n^{\text{th}}$ -order mode at  $\lambda_{775}$ , respectively.  $\theta(x, y)$  shows the transverse distribution of the nonlinear material: it equals 1 within the nonlinear polymer and 0 outside of it. Since  $\theta(x, y)$  is typically an even function of  $x$  ( $x = 0$  at waveguide's vertical line of symmetry),  $\Psi_{n, 775}$  must also be an even function of  $x$ ; otherwise,  $\Phi$  becomes zero. The lowest orders satisfying both this and  $n > m$  conditions are  $m = 0$ ,  $n = 2$ , on which we focus from now on. The normalized small-signal SHG conversion efficiency  $\eta$  is related to fundamental power  $P_{1550}$ , SHG power  $P_{775}$ , and waveguide length  $L$  by

$$\eta = P_{775}/(P_{1550}L)^2 = 8\pi^2 d_{\text{eff}}^2 \Phi / \left[ (n_{\text{eff}}^{m, 1550})^3 \lambda_{1550}^2 \epsilon_0 c \right]. \quad (3)$$

### 3. Investigation of a Single Channel Waveguide

We first consider a simple single channel waveguide with upper cladding made of a nonlinear polymer, shown in Fig. 1. The waveguide's lower cladding is a  $3.5\text{-}\mu\text{m}$ -thick layer of thermally-grown silicon dioxide ( $\text{SiO}_2$ ), which provides sufficient mode isolation from the Si substrate. We find from Sellmeier equation [33] the refractive indices of 1.998 (1.979) for stoichiometric SiN, i.e.,  $\text{Si}_3\text{N}_4$ , core and 1.454 (1.450) for  $\text{SiO}_2$  lower cladding at 775 nm (1550 nm) wavelength and assume index of 1.46 for a generic nonlinear polymer. In effective-index and mode-profile calculations, the polymer nonlinearity is neglected.

We model the entire waveguide structure of Fig. 1 by RSoft / Synopsys BeamPROP software, which uses finite-difference beam propagation method (FD-BPM) [34]. We start with a typical SiN waveguide with dimensions  $1\text{ }\mu\text{m} \times 0.32\text{ }\mu\text{m}$  ( $W \times H$ ), which does not require growing thick SiN films. It supports single 1550-nm and three 775-nm spatial modes. The mode profiles at 1550 nm and 775 nm are shown in Fig. 2, where TE corresponds to the horizontally-polarized (non-zero  $E_x$ ) and TM corresponds to the vertically-polarized (non-zero  $E_y$ ) electric field.

Next, we vary the width  $W$  and height  $H$  of the waveguide to achieve modal phase-matching separately for TE- and TM-polarized cases [35], with the results shown in Fig. 3. As can be seen in Fig. 3, phase-matching for TM polarization can be obtained by varying either width or height of the SiN core, whereas phase-matching for TE polarization can only be obtained by varying the waveguide width. The values of width  $W$  and height  $H$  corresponding to the phase-matched condition, as well as the resulting values of the effective area  $A_{\text{eff}}$  of SHG interaction are summarized in Table 1 for both TE- and TM-polarized cases. The results in Table 1 indicate that in a single-core waveguide structure the effective area  $A_{\text{eff}}$  of SHG interaction is too large ( $\sim 200\text{ }\mu\text{m}^2$ ) to yield an efficient nonlinear process. The reason for this is the fact that all three lobes of the 2<sup>nd</sup>-order SHG mode overlap with the fundamental wave in the nonlinear polymer cladding region. Compared to the

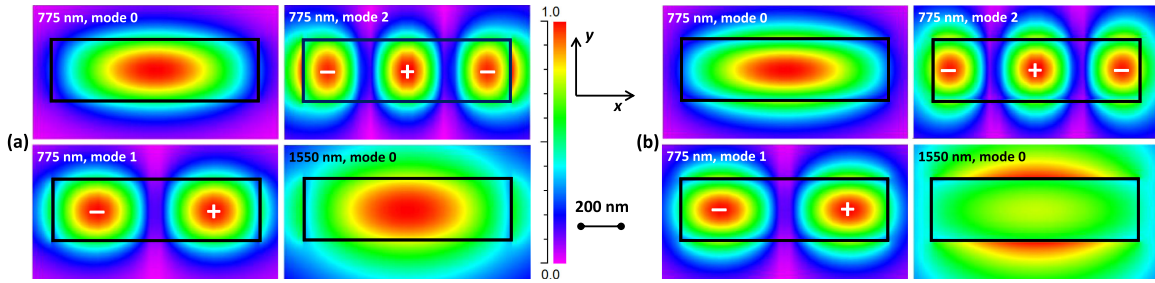


Fig. 2. 775-nm and 1550-nm mode profiles for (a) TE-polarized ( $|E_x|$  is shown) and (b) TM-polarized ( $|E_y|$  is shown) cases in a  $1\ \mu\text{m} \times 0.32\ \mu\text{m}$  single channel waveguide. Black rectangles show the border of SiN core. “ $\pm$ ” symbols indicate relative signs of different lobes.

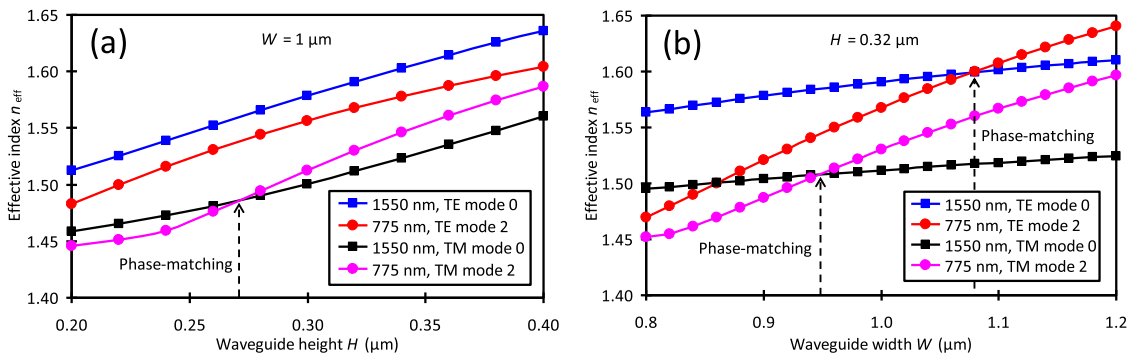


Fig. 3. Obtaining modal phase-matching condition of Eq. (1) by varying single channel waveguide’s (a) height  $H$  or (b) width  $W$ .

TABLE 1  
Single channel waveguide dimensions resulting in phase matching, as well as the corresponding effective areas

Waveguide dimensions $W \times H$ ( $\mu\text{m}$ )	Polarization	Effective area $A_{\text{eff}}$ ( $\mu\text{m}^2$ )
$1.08 \times 0.320$	TE	234
$1.00 \times 0.275$	TM	203
$0.95 \times 0.320$	TM	210

central lobe, the outer lobes provide opposite-sign contribution to the overlap integral  $\Phi$  of Eq. (2), largely canceling the central-lobe’s contribution and greatly reducing  $\Phi$  (and, hence, increasing  $A_{\text{eff}}$ ). To maximize the overlap integral, it would be highly desirable to reduce the contribution of the outer lobes to  $\Phi$  by reducing either their overlap with the fundamental wave or their overlap with the nonlinear material, while keeping the contribution of the central lobe intact. As we will see in the next Section, this can be achieved in a double-core waveguide structure (slot waveguide).

#### 4. Investigation of a Slot Waveguide

Slot waveguide consists of two channel cores of high refractive index, separated by a narrow gap (slot). The width of the low-index slot is normally less than the decay length of the field extending from the cores [36]. One of the advantages of the slot waveguide is the wide range of dispersion engineering realizable with it [37], [38]. Perhaps, its even more important advantage is the possibility of a significant electric-field enhancement in the slot region due to the discontinuity

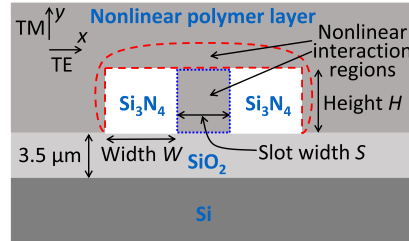


Fig. 4. Schematic of the slot waveguide with two SiN cores. Nonlinear  $\chi^{(2)}$  interaction occurs within the slot region with blue dotted-line border and within the upper-cladding region with red dashed-line border.

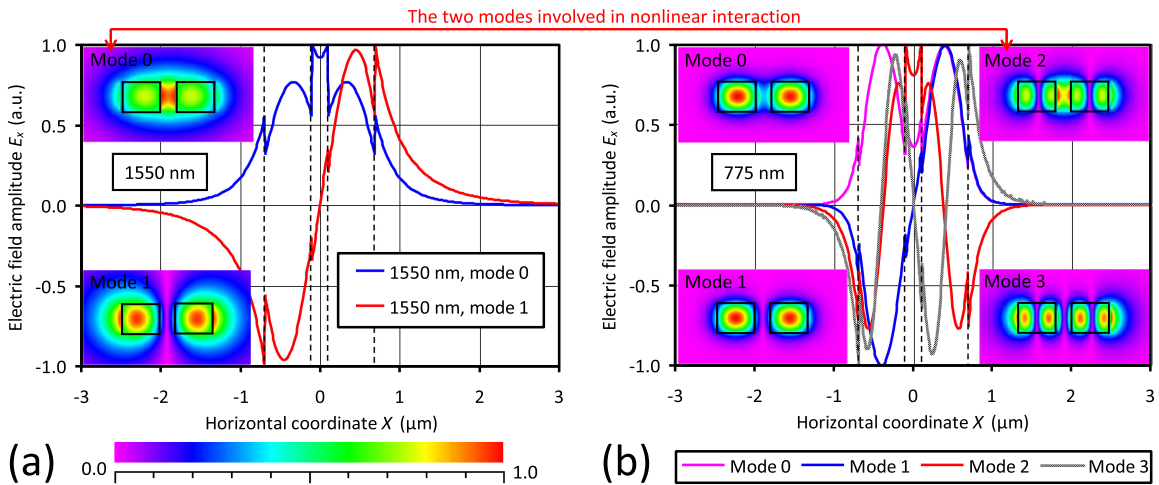


Fig. 5. TE mode profiles for (a) 1550 nm and (b) 775 nm beams. Black boxes (dashed lines) in the inserts (line graphs) show the borders of the SiN cores.

of the electric field at the slot-core interface [39], [40]. When the slot is filled by a nonlinear polymer material, this field enhancement can be used for nonlinear-optical applications: silicon-organic hybrid double-slot waveguides [8] and hetero-slot waveguides consisting of SiN and aluminum nitride [41] were proposed for  $\chi^{(2)}$  nonlinear processes in mid-infrared range. In this Section, we study a simple single-slot waveguide design and show its suitability for SHG by achieving phase matching and maximizing nonlinear overlap integral through optimization of waveguide geometry. We also describe the robustness of this design with respect to bending with reasonable radii down to  $\sim 150 \mu\text{m}$ , which permits its use in microresonators.

#### 4.1 Design and Optimization

We model and optimize the hybrid slot waveguide structure of Fig. 4, where upper cladding made of a nonlinear polymer also extends into the slot between the two SiN channel waveguides. We concentrate on the TE mode (horizontally-polarized electric field), because its electric field is significantly enhanced in the slot region, compared to the TM mode.

Figure 5 shows the TE spatial modes supported by the slot waveguide with width  $W = 589 \text{ nm}$ , height  $H = 450 \text{ nm}$ , and slot width  $S = 200 \text{ nm}$ : 2 at 1550 nm and 4 at 775 nm. These modes can be related to symmetric and anti-symmetric superpositions of the similar modes of the two distant channel waveguides. When the two channels are moved close to each other, their coupling makes these superpositions non-degenerate. In the symmetric (even-order) modes the fields from the two channels add in phase in the slot region. We will consider interaction between  $m = 0$  mode

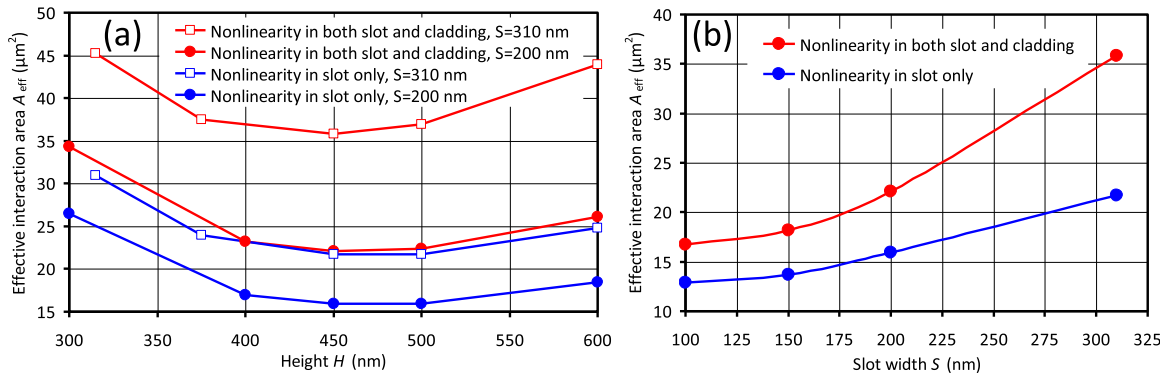


Fig. 6. Dependence of the effective interaction area  $A_{\text{eff}}$  (a) on waveguide height  $H$  for fixed slot widths  $S = 200 \text{ nm}$  and  $S = 310 \text{ nm}$  and (b) on slot width  $S$  for optimum waveguide height  $H = 450 \text{ nm}$ . At every point, the channel width  $W$  is chosen to satisfy the phase-matching condition.

at 1550 nm and  $n = 2$  mode at 775 nm, for both of which the field in the nonlinear slot is strongly enhanced. Note that the negative-sign outer lobes of the 2<sup>nd</sup>-order 775-nm mode do not extend into the field-enhanced slot region and overlap only with weak tails of the 0<sup>th</sup>-order 1550-nm mode, which limits their negative impact on  $\Phi$ . We optimize two cases having same linear (effective indices, mode structure), but different nonlinear (overlap  $\Phi$ ) properties: a) nonlinear polymer confined only to the slot region, whereas the upper cladding is made of a strictly linear polymer; b) nonlinear polymer extending to both slot and upper cladding regions.

We start optimization of the slot waveguide geometry from the parameters of the optimum single channel waveguide for the TE case ( $1.08 \mu\text{m} W \times 0.32 \mu\text{m} H$ ), divide its width by two, and insert a  $0.1\text{--}0.5\text{-}\mu\text{m}$  gap between the two halves (limited by practical fabrication constraints on the lower side [42] and by decreasing nonlinear overlap on the higher side). The height of the waveguide corresponds to the thickness of SiN layer, growth of which is limited by the high tensile stress [43]. To optimize, we independently vary the waveguide height  $H$  and slot width  $S$ , choose each channel width  $W$  to satisfy the phase-matching condition for given  $H$  and  $S$ , and then finally calculate the overlap integral of Eq. (2) for each combination. Figure 6a shows the resulting effective interaction area  $A_{\text{eff}}$  as a function of waveguide height  $H$  for two values of slot width,  $S = 200 \text{ nm}$  and  $S = 310 \text{ nm}$ . In all cases, the optimum height is near 450 nm. Next, we vary the slot width  $S$  while keeping the height  $H$  at 450 nm (the width  $W$  is always adjusted to obtain the phase matching) and plot the resulting values of  $A_{\text{eff}}$  in Fig. 6b. We see that the effective area monotonically increases with slot width, initially very slowly (in  $100\text{--}150\text{-nm}$  region) and then linearly (after  $\sim 175 \text{ nm}$ ). Even though the smallest slot widths offer marginally smaller  $A_{\text{eff}}$  values, etching of narrow slots with high-aspect-ratio ( $100 \text{ nm wide} \times 450 \text{ nm deep}$ ) is very challenging. We choose  $S = 200 \text{ nm}$  as the smallest practical slot width, and, according to Fig. 6b, it yields  $A_{\text{eff}}$  within 20% from its global minimum value. For the optimum combination of height  $H = 450 \text{ nm}$  and slot width  $S = 200 \text{ nm}$ , the phase matching is achieved at channel width  $W = 589 \text{ nm}$ .

Figure 7a shows effective indices  $n_{\text{eff}}$  of various 775-nm and 1550-nm modes versus slot width  $S$  at optimum values of  $H = 450 \text{ nm}$  and  $W = 589 \text{ nm}$ . The curves for 0<sup>th</sup>-order fundamental mode and 2<sup>nd</sup>-order SHG mode almost overlap in a wide region around design value of  $S = 200 \text{ nm}$ , indicating nearly non-critical phase-matching that is robust to fabrication errors.

#### 4.2 Results and Discussion

The results of the optimization are summarized in Table 2. For polymer that fills both the slot and the upper cladding, we have obtained the minimum effective area  $A_{\text{eff}} = 22.1 \mu\text{m}^2$ . The effective area can be further reduced by using polymer only in the slot region and filling the rest of the upper cladding by a linear polymer (or by  $\text{SiO}_2$ ). In that case, the overlap-reducing contribution of the

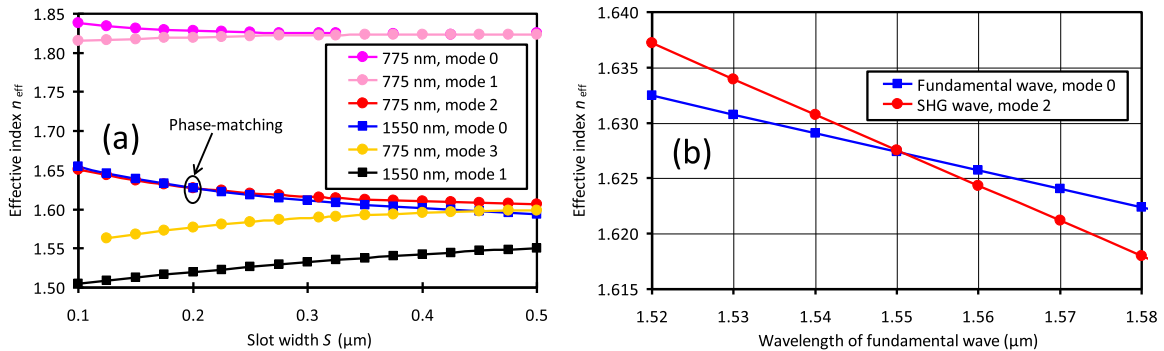


Fig. 7. (a) Slot-width dependence of the effective indices of all supported TE modes of the waveguide with optimum height  $H = 450$  nm and width  $W = 589$  nm. (b) Effective refractive index of the optimum slot waveguide ( $W = 589$  nm,  $H = 450$  nm,  $S = 200$  nm) as a function of wavelength.

TABLE 2

Optimized slot waveguide dimensions resulting in both phase-matching and minimized effective areas

Optimized waveguide dimensions $W \times H \times S$ (μm)	Polarization	Effective interaction area $A_{\text{eff}}$ (μm <sup>2</sup> )	
		Nonlinearity in both slot and cladding	Nonlinearity in slot region only
0.589 × 0.45 × 0.20	TE	22.1	15.9
0.5 × 0.3 × 0.33	TM	404	308

two negative outer lobes of the 2<sup>nd</sup>-order SHG mode (red curve in Fig. 5b) completely vanishes [there is no nonlinear polymer, i.e.,  $\theta(x, y) = 0$ , in the region of the outer lobes], and the resulting effective area is reduced to  $A_{\text{eff}} = 15.9 \mu\text{m}^2$ . For comparison, we also show the optimized values of the effective area for TM-polarized case. Unlike TE wave, TM wave does not benefit from the field enhancement in the slot, and its effective area is comparable (more precisely, somewhat larger) than that in the single channel waveguide case. The optimized TE case compares favorably to typical values of  $A_{\text{eff}} \approx 25 \mu\text{m}^2$  and  $A_{\text{eff}} \approx 60 \mu\text{m}^2$  for SHG in single- and two-mode [29], [30] PPLN waveguides, respectively. The nonlinear polymers have high  $d_{\text{eff}} \sim 100\text{--}500 \text{ pm/V}$  [7], [44]. Even for a conservative value of  $d_{\text{eff}} \sim 20 \text{ pm/V}$ , Eq. (3) yields conversion efficiency  $\eta = 730\% / \text{W} / \text{cm}^2$  for TE case with  $A_{\text{eff}} = 15.9 \mu\text{m}^2$ , which is an order of magnitude more efficient than single-mode PPLN ( $\eta \approx 70\% / \text{W} / \text{cm}^2$ ). With low SiN loss (<0.5 dB/cm) [2], cm-scale waveguides are feasible.

Figure 7b shows the wavelength dependence of the effective index for the optimum slot waveguide in the vicinity of the phase-matching wavelength. Detuning from the design wavelength changes the effective index by  $\Delta n_{\text{eff}} \approx 0.015$  per 100 nm of wavelength change. This can be used to estimate the shift of the phase-matched wavelength owing to fabrication errors.

#### 4.3 Effect of Bending

To explore the use of the hybrid SiN / polymer slot waveguide in microrings, we analyze the effect of bending on the optimum slot waveguide ( $W = 589$  nm,  $H = 450$  nm,  $S = 200$  nm) by employing the simulated bend method of RSoft BeamPROP [34]. This method maps a bent waveguide onto a straight waveguide by a coordinate transformation. The waveguide length is taken as a quarter arc with a radius  $R = c / (2\pi n_{\text{eff}} \Delta\nu) = 146.7 \mu\text{m}$ , corresponding to a microring with free spectral range  $\Delta\nu = 200$  GHz and phase-matched effective index  $n_{\text{eff}} = 1.6274$ . We consider TE case only and find that bending slightly shifts the phase-matching wavelength. This shift can be compensated by either a small change in the waveguide dimensions (e.g., ~3 nm change in channel width  $W$ ) or by a slight (<10 nm) shift of the slot position towards the center of curvature [45], as shown in Fig. 8a. In Fig. 8a the slot position is varied with respect to the center of the structure in a range

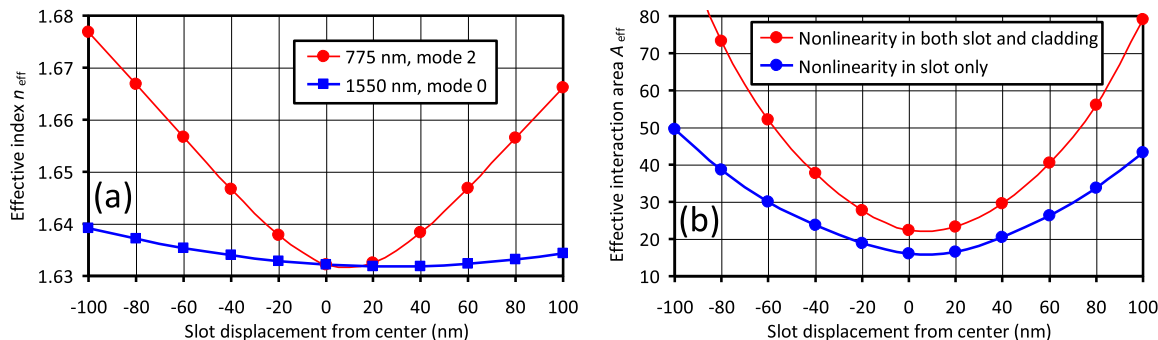


Fig. 8. Effects of the slot position in a bent waveguide (a) on the effective indices  $n_{\text{eff}}$  of the interacting modes and (b) on the effective interaction area  $A_{\text{eff}}$ .

from  $-100$  nm to  $100$  nm, which corresponds to the movement towards outside and inside of the bend, respectively.

Such shift of the slot does not significantly impact the effective area  $A_{\text{eff}}$  of Eq. (2), as shown in Fig. 8b.  $10$ -nm shift of the slot reduces  $A_{\text{eff}}$  by about  $2.1\%$  when the polymer is only in the slot region and by about  $1.7\%$  when the polymer is in both slot and upper cladding regions. These results prove the robustness of the hybrid SiN / polymer waveguide to bending.

## 5. Conclusions

We have discussed the design and optimization of a SiN waveguide with polymer cladding layer to generate second harmonic of a  $1550$ -nm wave. We have shown that a single channel waveguide can be optimized to achieve the phase-matching condition between  $0^{\text{th}}$ -order fundamental and  $2^{\text{nd}}$ -order second-harmonic modes, but the effective nonlinearity in this case is very low due to a poor nonlinear overlap integral. In contrast, an optimized slot waveguide with nonlinear polymer filling either the slot or both the slot and upper cladding has an order-of-magnitude higher nonlinear overlap integral. We have shown that both phase-matching condition and the nonlinear overlap integral are robust with respect to fabrication errors and to waveguide bending with radii as small as  $\sim 150 \mu\text{m}$ , which is promising for the development of waveguide- and microresonator-based nonlinear photonic integrated circuits. The conversion between a fundamental Gaussian beam and a higher-order waveguide mode can be easily done by a phase plate or a spatial light modulator [29], [30].

## References

- [1] B. J. Eggleton *et al.*, "Chalcogenide photonics," *Nature Photon.*, vol. 5, pp. 141–148, 2011.
- [2] D. J. Moss *et al.*, "New CMOS-compatible platforms based on silicon nitride and Hydex for nonlinear optics," *Nature Photon.*, vol. 7, pp. 597–607, 2013.
- [3] F. Da Ros *et al.*, "Characterization and optimization of a high-efficiency AlGaAs-on-Insulator-based wavelength converter for 64- and 256-QAM signals," *J. Lightw. Technol.*, vol. 35, no. 17, pp. 3750–3757, Sep. 2017.
- [4] Z. Tong *et al.*, "Noise performance of a frequency non-degenerate phase-sensitive amplifier with un-equalized inputs," *Opt. Lett.*, vol. 36, pp. 722–724, 2011.
- [5] Z. Tong *et al.*, "Modeling and measurement of the noise figure of a cascaded non-degenerate phase-sensitive parametric amplifier," *Opt. Exp.*, vol. 18, pp. 14820–14835, 2010.
- [6] F. Flaminio *et al.*, "Photonic quantum information processing: A review," *Rep. Prog. Phys.*, vol. 82, 2019, Art. no. 016001.
- [7] J. Leuthold *et al.*, "Silicon organic hybrid technology – a platform for practical nonlinear optics," *Proc. IEEE*, vol. 97, pp. 1304–1316, 2009.
- [8] L. Alloatti *et al.*, "Second-order nonlinear silicon-organic hybrid waveguides," *Opt. Exp.*, vol. 20, pp. 20506–20515, 2012.
- [9] C. H. Henry *et al.*, "Low loss SiN-SiO<sub>2</sub> optical waveguides on Si," *Appl. Opt.*, vol. 26, pp. 2621–2624, 1987.
- [10] W. Stutius and W. Streifer, "Silicon nitride films on silicon for optical waveguides," *Appl. Opt.*, vol. 16, pp. 3218–3222, 1977.

- [11] L. Yi *et al.*, "Characterization of hybrid InP-TriPleX photonic integrated tunable lasers based on silicon nitride ( $\text{Si}_3\text{N}_4/\text{SiO}_2$ ) microring resonators for optical coherent system," *IEEE Photon. J.*, vol. 10, no. 3, Jun. 2018, Art. no. 1400108.
- [12] C. J. Cullen *et al.*, "Thin-film silicon nitride on electro-optic materials for a novel modulator architecture," in *Proc. IEEE Res. Appl. Photon. Defense Conf.*, Miramar Beach, FL, USA, Aug. 2018, paper ThC2.6.
- [13] K. Ikeda *et al.*, "Thermal and Kerr nonlinear properties of plasma-deposited silicon nitride/ silicon dioxide waveguides," *Opt. Exp.*, vol. 16, pp. 12987–12994, 2008.
- [14] A. R. Johnson *et al.*, "Octave-spanning coherent supercontinuum generation in a silicon nitride waveguide," *Opt. Lett.*, vol. 40, pp. 5117–5120, 2015.
- [15] K. J. A. Ooi *et al.*, "Pushing the limits of CMOS optical parametric amplifiers with USRN:  $\text{Si}_7\text{N}_3$  above the two-photon absorption edge," *Nature Commun.*, vol. 8, 2017, Art. no. 13878.
- [16] H. Guo *et al.*, "Mid-infrared frequency comb via coherent dispersive wave generation in silicon nitride nanophotonic waveguides," *Nature Photon.*, vol. 12, pp. 330–335, 2018.
- [17] H. Zhao *et al.*, "Stimulated Raman spectroscopy of analytes evanescently probed by a silicon nitride photonic integrated waveguide," *Opt. Lett.*, vol. 43, pp. 1403–1406, 2018.
- [18] M. Yang *et al.*, "An octave-spanning optical parametric amplifier based on a low dispersion silicon rich nitride waveguide," *IEEE J. Sel. Topics Quantum Electron.*, vol. 24, no. 6, Nov./Dec. 2018, Art. no. 8300607.
- [19] M. Cazzanelli *et al.*, "Second-harmonic generation in silicon waveguides strained by silicon nitride," *Nature Mater.*, vol. 11, pp. 148–154, 2012.
- [20] J. S. Levy *et al.*, "Harmonic generation in silicon nitride ring resonators," *Opt. Exp.*, vol. 19, pp. 11415–11421, 2011.
- [21] R. E. P. de Oliveira and C. J. S. de Matos, "Quasi-phase-matched second harmonic generation in silicon nitride ring resonators controlled by static electric field," *Opt. Exp.*, vol. 21, pp. 32690–32698, 2013.
- [22] A. Farsi *et al.*, "Large effective  $\chi^{(2)}$  nonlinearity via coherent photon conversion on a  $\text{Si}_3\text{N}_4$  chip," in *Proc. Conf. Lasers Electro-Opt.*, San Jose, CA, USA, May 2017, paper FTu3D.5.
- [23] S. V. Rao *et al.*, "Nonlinear frequency conversion in semiconductor optical waveguides using birefringent, modal and quasi-phase-matching techniques," *J. Opt. A, Pure Appl. Opt.*, vol. 6, pp. 569–584, 2004.
- [24] M. Annamalai *et al.*, "Phase-sensitive multimode parametric amplification in parabolic-index waveguide," *IEEE Photon. Technol. Lett.*, vol. 24, no. 21, pp. 1949–1952, Nov. 2012.
- [25] Y. B. Kwon and M. Vasilyev, "Mode-selective frequency up-conversion in a  $\chi^{(2)}$  waveguide," *Proc. SPIE*, vol. 8964, 2014, Art. no. 8964ON.
- [26] M. Annamalai *et al.*, "Spatial modes of phase-sensitive parametric image amplifiers with circular and elliptical Gaussian pumps," *Opt. Exp.*, vol. 19, pp. 26710–26724, 2011.
- [27] M. Annamalai *et al.*, "Compact representation of the spatial modes of a phase-sensitive image amplifier," *Opt. Exp.*, vol. 21, pp. 28134–28153, 2013.
- [28] M. Vasilyev and Y. B. Kwon, "Spatial-mode-selective quantum frequency conversion in nonlinear waveguides," *Proc. SPIE*, vol. 9505, 2015, Art. no. 95050O.
- [29] Y. B. Kwon *et al.*, "Experimental demonstration of spatial-mode-selective frequency up-conversion in a multimode  $\chi^{(2)}$  waveguide," in *Proc. Conf. Lasers Electro-Opt.*, San Jose, CA, USA, Jun. 2016, paper STh3P.4.
- [30] Y. B. Kwon *et al.*, "Single-photon-level spatial-mode-selective frequency up-conversion in a multimode  $\chi^{(2)}$  waveguide," in *Proc. Conf. Lasers Electro-Opt.*, San Jose, CA, USA, May 2017, paper FF2E.1.
- [31] S. Das *et al.*, "Hybrid silicon-nitride / polymer waveguide for nonlinear-optics applications," in *Proc. Conf. Lasers Electro-Opt.*, San Jose, CA, USA, May 2018, paper JTU2A.77.
- [32] S. Das *et al.*, "Robustness of second-harmonic generation in a hybrid SiN / polymer waveguide," in *Proc. IEEE Photon. Soc. Res. Appl. Photon. Defense Conf.*, Miramar Beach, FL, USA, Aug. 2018, paper ThC2.7.
- [33] T. Báák, "Silicon oxynitride; A material for GRIN optics," *Appl. Opt.*, vol. 21, pp. 1069–1072, 1982.
- [34] BeamPROP software by RSoft / Synopsys; description is available online at <https://www.synopsys.com/optical-solutions/rsoft/passive-device-beamprop.html>
- [35] J. M. Chavez Boggio *et al.*, "Dispersion engineered silicon nitride waveguides by geometrical and refractive-index optimization," *J. Opt. Soc. Amer. B*, vol. 31, pp. 2846–2857, 2014.
- [36] Q. Xu *et al.*, "Experimental demonstration of guiding and confining light in nanometer-size low-refractive-index material," *Opt. Lett.*, vol. 29, pp. 1626–1628, 2004.
- [37] M. Fujii, J. Leuthold, and W. Freude, "Dispersion relation and loss of subwavelength confined mode of metal-dielectric-gap optical waveguides," *IEEE Photon. Technol. Lett.*, vol. 21, no. 6, pp. 362–364, Mar. 2009.
- [38] L. Zhang *et al.*, "Flattened dispersion in silicon slot waveguides," *Opt. Exp.*, vol. 18, pp. 20529–20534, 2010.
- [39] V. R. Almeida *et al.*, "Guiding and confining light in void nanostructure," *Opt. Lett.*, vol. 29, pp. 1209–1211, 2004.
- [40] H. Tian *et al.*, "Dynamics of nanoparticles trapped on an integrated slot waveguide with a high index contrast," in *Proc. OSA Opt. Life Sci. Cong.*, San Diego, CA, USA, Apr. 2017, paper OTS1D.4.
- [41] S. Kim and M. Qi, "Broadband second-harmonic phase-matching in dispersion engineered slot waveguides," *Opt. Exp.*, vol. 24, pp. 773–786, 2016.
- [42] C. Koos *et al.*, "Nonlinear high index-contrast waveguides with optimum geometry," in *Proc. OSA Topical Meeting*, Quebec City, QC, Canada, Sep. 2007, paper JWA2.
- [43] A. Gondarenko, J. S. Levy, and M. Lipson, "High confinement micron-scale silicon nitride high Q ring resonator," *Opt. Exp.*, vol. 17, 2009, Art. no. 11366.
- [44] J. Luo *et al.*, "Efficient wafer-scale poling of electro-optic polymer thin films on soda-lime glass substrates: Large second-order nonlinear coefficients and exceptional homogeneity of optical birefringence," *Opt. Mater. Exp.*, vol. 7, pp. 1909–1916, 2017.
- [45] P. A. Anderson, B. S. Schmidt, and M. Lipson, "High confinement in silicon slot waveguides with sharp bends," *Opt. Exp.*, vol. 14, pp. 9197–9202, 2006.